Accepted Manuscript

A hierarchical porous microstructure for improving long-term stability of $Ni_{1-x}Cu_x$/SDC anode-supported IT-SOFCs fueled with dry methane

Zhicheng Wang, Siqi Wang, Shiyan Jiao, Wenjian Weng, Kui Cheng, Bin Qian, Hailin Yu, Yimin Chao

PII: S0925-8388(17)30246-3

DOI: 10.1016/j.jallcom.2017.01.212

Reference: JALCOM 40579

To appear in: *Journal of Alloys and Compounds*

Received Date: 6 May 2016

Revised Date: 5 January 2017

Accepted Date: 19 January 2017

Please cite this article as: Z. Wang, S. Wang, S. Jiao, W. Weng, K. Cheng, B. Qian, H. Yu, Y. Chao, A hierarchical porous microstructure for improving long-term stability of $Ni_{1-x}Cu_x$/SDC anode-supported IT-SOFCs fueled with dry methane, *Journal of Alloys and Compounds* (2017), doi: 10.1016/j.jallcom.2017.01.212.

A hierarchical porous microstructure for improving long-term stability of $Ni_{1-x}Cu_x$/SDC anode-supported IT-SOFCs fueled with dry methane

Zhicheng Wang[a, *], Siqi Wang[a], Shiyan Jiao[a], Wenjian Weng[b], Kui Cheng[b], Bin Qian[a], Hailin Yu[a], Yimin Chao[c, **]

[a]Department of Physics and Electronic Engineering, Changshu Institute of Technology, Changshu 215500, PR China

[b]School of Materials Science and Engineering, Zhejiang University, Hangzhou 310027, PR China

[c]School of Chemistry, University of East Anglia, Norwich NR4 7TJ, UK

Abstract

A series of $Ni_{1-x}Cu_x$/Sm-doped ceria ($Ni_{1-x}Cu_x$/SDC) anodes have been prepared through introducing a soluble pore former with the co-pressing and co-sintering process. Uniform hierarchical porous microstructures are formed in $Ni_{0.9}Cu_{0.1}$/SDC anode with interconnected large pores of 2~5 μm and 100~300 nm small pores on the wall. The solid oxide fuel cell (SOFC) based on such anode exhibits exceptional electrochemical catalytic activity for dry CH_4 oxidation and a maximum power density of 379 mW cm^{-2} is acquired at 600°C. Durability test results show only 2.4% power density drop is observed after 72 h operation under a constant cell voltage of 0.5 V. The results have demonstrated that the optimization of anode microstructures is an effective way to improve the performance and long-term stability of $Ni_{1-x}Cu_x$ alloy-based anode-supported SOFC.

Keywords: Hierarchical porous microstructure; $Ni_{1-x}Cu_x$ alloy-based anode; Solid oxide fuel cells; methane; long-term stability.

* Corresponding author. Fax: +86 512 52251552. E-mail address: wzc877@zju.edu.cn (Z. Wang)

** Corresponding co-author. Tel.: +44 1603 59 3146; Fax: +44 1603 59 2003. E-mail address: Y.Chao@uea.ac.uk (Y. Chao)

1. Introduction

Intermediate temperature solid oxide fuel cells (IT-SOFCs) offer a clean and environmentally friendly technology to convert chemical energy directly into electricity with high efficiency and low pollution at 800°C to 600°C or even lower temperature region [1-5]. One of the major advantages of IT-SOFCs over other types of fuel cells is the excellent fuel flexibility, which means SOFCs possess the ability to handle more convenient hydrocarbon fuels, for direct oxidation without internal or external reforming processes [6-10]. The direct electrochemical oxidation is to render the SOFCs with high conversion efficiency, relatively simple system design, and avoiding many problems associated with the generation and storage of hydrogen [11-13].

As the most commonly used anode materials for SOFCs, the low-cost Ni-cermet anodes possess excellent electrochemical catalytic activity for fuel oxidation, high electrical conductivity, as well as good stability and compatibility with electrolyte materials. However, when the typical Ni-based anode is used directly in a dry hydrocarbon environment, the corresponding SOFCs exhibit a performance slightly increased initially, and then degraded with elongated operation time. This is owing to that Ni is also an active catalyst for C-C bonds formation. The produced carbon forms carbon deposits that cover the catalytic active sites and reduce the length of triple-phase boundaries (TPBs). Moreover, the carbon deposition can block the anode pores, increase gas diffusion resistance and disrupt the anode structure eventually [10, 14-18]. Therefore, anode materials with appropriate microstructure, high catalytic

activity, effective carbon deposition inhibition, and long-term stability at intermediate temperatures are critical for direct oxidation of hydrocarbon fuels in SOFCs.

In order to avoid or minimize carbon deposition of traditional Ni-based anodes, many studies have focused on small part substitution of Cu in Ni-based anode to improve the catalytic activity for the electrochemical oxidation and reduce the carbon deposition. This is because of Cu is relatively inert for the formation of C-C bonds although the catalytic activity of Cu is lower than that of Ni for the electrochemical oxidation of the fuel [19]. One approach is to modify the Ni-cermet anode with Cu through the wet impregnation technique. When Cu nanoparticles are uniformly distributed in the porous Ni/Sm-doped ceria (Ni/SDC) matrix, the cell stability in dry methane is significantly improved [20]. In literature, the Cu-ceria composites have been co-impregnated into the Ni/yttria-stabilized zirconia (Ni/YSZ) supported outer layer, resulted in a Ni/YSZ electroactive inner layer exhibiting high electrochemical performance without anode coking for the direct operation on ethanol [21]. Such wet impregnation/infiltration has been proved to be a very effective approach to fabricate and/or optimize SOFC anodes to obtain better performance and stability. However, too many repeated cycles are required to get the desired impregnation loading and microstructures, which lead to the complexity and instability for fabrication [22-25].

Replacing Ni with $Ni_{1-x}Cu_x$ alloy for hydrocarbon utilization is another approach [26-29]. The co-sintering is the most commonly used method to prepare the $Ni_{1-x}Cu_x$ alloy-based anode. A $Ni_{0.95}Cu_{0.05}$/SDC anode-supported cell has been prepared by co-sintering and operated with hydrocarbon at 600°C. Although pretty good

performance with a power density of 338 mW cm^{-2} has been achieved, carbon has still formed on the anode due to the low concentration of Cu in the solid solution [20]. C. M. Grgicak et al. [27] have demonstrated that the $Ni_{1-x}Cu_x$ alloy is insufficient to suppress carbon formation in $Ni_{1-x}Cu_x$-YSZ anode prepared by sintering even with x up to 0.21. Interestingly, Kim et al. [29] fabricated a $Ni_{0.2}Cu_{0.8}$ alloy based anode by dually impregnating Cu and Ni nitrate solution into a porous YSZ anode followed by reduction at 900°C. The single cell with such anode has shown good thermal stability and operation stability in methane. This implies that improving the $Ni_{1-x}Cu_x$ alloy-based anode microstructure is an effective approach for directly utilizing hydrocarbon when the x of Cu in the solid solution is lower than 0.21.

In literature, the studies of $Ni_{1-x}Cu_x$ alloy-based anode microstructure optimization are mainly focused on the wet impregnation method [22, 29] and few works have been done by introducing the hierarchical porous microstructure in the anode. In order to simply the complex multiple fabrication process of the wet impregnation, in this work, the conventional fabrication techniques by the co-pressing and co-sintering process are modified through using a soluble pore former and a novel $Ni_{1-x}Cu_x$ alloy-based anode with hierarchical porous microstructure is successfully fabricated. Such an anode is expected to have longer TPBs and possesses excellent electrochemical catalytic activity and coking tolerance for dry CH_4 oxidation. The $Ni_{1-x}Cu_x$/SDC-supported cells have been tested with dry CH_4 as fuel and the cell stability of direct oxidation of dry CH_4 is to be discussed as well.

2. Experimental details

2.1. Anodes and fuel cell preparation

A series of nanosized $Ni_{1-x}Cu_xO$ (x=0.1, 0.15, 0.2) powders were synthesized by the glycine-nitrate combustion process [30-31] with stoichiometric amounts of $Ni(NO_3)_2 \cdot 6H_2O$ (99.9%), $Cu(NO_3)_2 \cdot 6H_2O$ (99.9%) and glycine (NH_2-CH_2-COOH). The SDC and SSC ($Sm_{0.5}Sr_{0.5}CoO_3$) powders were also prepared with the corresponding nitrates. The anode materials with 65 wt.% $Ni_xCu_{1-x}O$ powder and 35 wt.% SDC powder, while the cathode materials with 70 wt.% SSC powder and 30 wt.% SDC powder, were mixed by wet ball-milling for 72h with ethanol as liquid medium and then dried in the drying oven at 50 °C.

In order to fabricate a single $Ni_{1-x}Cu_x$/SDC anode-supported cell, the anode materials were mixed with 5 wt.% ethylcellulose in the ethanol by ball-milling for at least 6h to make ethylcellulose dissolved completely. After vacuum drying at room temperature, the mixture was pressed at 100 MPa in the die. Then, SDC powder was added and co-pressed at 200 MPa to form a bilayer disc with a diameter of 15 mm and a thickness of about 1 mm. The bilayer disc was sintered at 1350°C for 4h. The porous cathode was prepared on the electrolyte surface by spin-coating with a suspension consisting of cathode material, ethylcellulose and ethanol, followed by sintering at 950°C for 2h in air. All the Ni_xCu_{1-x}/SDC supported cells were fabricated with the same processes to avoid cathodic polarization resistance variations.

2.2. Characterization and cell testing

The phase of anode material before and after reduction was characterized by

X-ray diffraction (XRD, Bruker) using Cu K_α radiation. Prior to the electrochemical test, the single cell was reduced in the flowing H_2 at 600°C for 4h. The cross-sectional microstructures of the prepared electrodes and cells were investigated by scanning electron microscope (SEM, SIGMA, ZEISS) and the copper distribution was detected with an attached energy dispersive spectroscopy (EDS). The anode porosity was characterized by Archimedes' density measurements and the conductivity was measured using the four-probe method after the $Ni_xCu_{1-x}O$/SDC cermet was reduced by H_2.

Each single cell was mounted onto a quartz tube using silver paste. The current collector was a Ag-mesh (Alfa Aesar，0.003 in) which was sintered on the both sides of cell and two silver wires (Alfa Aesar，0.01 in) were used as the leads for both electrodes. The anode side was fed with dry CH_4 at a flow rate of 60 mL min^{-1} and the cathode side worked in air atmosphere. A potentiostat (CHI760C, CH Instrument) was used to record the current density-voltage (*I-V*) curves and electrochemical impedance spectra. The AC impedance of the cell under open-circuit conditions was collected in the frequency range from 0.01 Hz to 100 kHz with the signal amplitude 5 mV. The carbon deposition was analyzed with EDS after electrochemical test.

3. Results and discussion

3.1. Structural characterization and morphologies

Fig.1 shows the XRD patterns of $Ni_{0.9}Cu_{0.1}O$/SDC cermet before the reduction and $Ni_{0.9}Cu_{0.1}$/SDC anode after the reduction under H_2. The XRD pattern (Fig. 1(a)) of the anode cermet shows diffraction peaks of both SDC and $Ni_{0.9}Cu_{0.1}O$, without

any other impurity peaks. The results indicate that there is no chemical reaction between $Ni_{0.9}Cu_{0.1}O$ and SDC during sintering. After reduction with H_2, the XRD pattern of the corresponding anode is shown in Fig. 1(b), the diffraction peaks of $Ni_{0.9}Cu_{0.1}$ alloy match the (111) and (200) characteristics of fcc structured Ni but shifted to lower angles, with no any residual Cu phase detected. The results have demonstrated the formation of pure $Ni_{0.9}Cu_{0.1}$ alloy.

Fig. 2(a) shows the cross-sectional microstructure of a single $Ni_{0.9}Cu_{0.1}$/SDC anode-supported cell with reduced anode. The single cell consists of ~35 μm SSC-SDC cathode, ~35 μm SDC electrolyte and ~500 μm anode. The crack-free dense SDC electrolyte layer bonds strongly to the porous anode substrate. The porous thin cathode shows good adhesion to the electrolyte and no obvious collapsed pores in it. The microstructure of the $Ni_{0.9}Cu_{0.1}$/SDC anode is shown in Fig. 2(b) and there are two types of pores can been observed inside the anode. The larger pores are 2-5 μm in diameter, which are interconnected within the structure. As shown in the inset in Fig. 2(b), the smaller pores are 100~300 nm in diameter, which are homogeneously distributed in the anode matrix. Such a hierarchical porous anode structure is ideal for application owing to the following two characteristics: the larger pores can promote rapid gas transport through the porous electrodes, while the smaller pores provide high surface areas for gas adsorption/desorption with more catalytically active sites for reactions [32].

Fig. 3 shows the cross-sectional microstructures (left) and corresponding EDS mapping of the copper distribution (right) of the $Ni_{1-x}Cu_x$/SDC anodes. It is obvious

that the morphology of the anode varies with the copper concentrations in $Ni_{1-x}Cu_x$ alloy. The $Ni_{0.9}Cu_{0.1}$/SDC anode shows a uniform hierarchical porous microstructure and the smaller pores are homogeneously distributed in the framework. The number of smaller pores gradually decreases with increasing copper content and almost disappears when x increased to 0.2. This result is consistent with the changing trend of the porosity in different anodes that is listed in Table 1. The EDS element mappings show that the copper is uniformly distributed in the $Ni_{0.9}Cu_{0.1}$/SDC anode but aggregates are observed with the increased concentration x. These trends are related with the size of alloy particle. C. M. Grgicak et al. [27] have reported that the alloy particle sizes increase with the increasing of the copper concentration in it. As shown in Table 1, the electrical conductivity of the anode can be improved with the larger alloy particle because the electrical conductivity is mainly attributed to the alloy particle connections and the larger alloy particle size leads to better electrical connection [33]. However, the larger particle size is against the formation of the uniform microstructure and the uniform phase distribution [34]. Meanwhile, the porosity of the microstructure is also affected by the alloy particle size in the anode [33], because the increasing of the alloy particle size may lead to reduced number of the smaller pores. These are undesirable effects that lead to the reduction of the active area for fuel oxidation.

3.2. Performance with dry CH_4 fuel

Fig. 4 shows the voltage and power density as a function of current density for $Ni_{1-x}Cu_x$/SDC anode-supported cells operated at different temperature with dry CH_4

as the fuel. The results are summarized in Table 2. It can be seen that the open circuit voltages (OCVs) of $Ni_{0.9}Cu_{0.1}$/SDC, $Ni_{0.85}Cu_{0.15}$/SDC and $Ni_{0.8}Cu_{0.2}$/SDC supported cells at 600°C are 0.915, 0.894 and 0.875 V, respectively. These results are all smaller than the theoretical value of 0.943 V when the methane is completely oxidized. Such a result implies that some side electrochemical reaction [35] may have occurred in the anode. On the other hand, the doped ceria electrolyte exhibits mixed ionic and electronic conduction due to partial reduction of Ce^{4+} into Ce^{3+} in the reducing atmosphere, which also leads to the decrease of the OCV of a SOFC [36]. Furthermore, it can be seen that the OCV of the SOFCs decreases with the increasing of Cu content. This is partly due to that the electrochemical catalytic activity of Cu is inferior to that of Ni for fuels [19] and the increasing content of Cu in anode leads to the decrease of catalytic activity of the alloy. In addition, Cu diffusion into ceria electrolyte further induces the transition from Ce^{4+} to Ce^{3+} [37] and the larger amount of Cu content leads to higher percentage of cerium in the +3 oxidation state, which results in the larger loss of the OCV.

The maximum power densities for $Ni_{0.9}Cu_{0.1}$/SDC, $Ni_{0.85}Cu_{0.15}$/SDC and $Ni_{0.8}Cu_{0.2}$/SDC supported cells at 600°C are 379, 337 and 273 mW cm^{-2}, respectively. The results show that the cell performance decreases with the increase of Cu content in $Ni_{1-x}Cu_x$ alloy at the same testing temperature. This is also due to the fact that the catalytic activity of Cu is inferior to that of Ni for the electrochemical oxidation of fuel [19]. Comparing the maximum power density of 338 mW cm^{-2} from our previous work on $Ni_{0.95}Cu_{0.05}$/SDC supported cell [20], the maximum power density of the

$Ni_{0.9}Cu_{0.1}$/SDC supported cell with the hierarchical pores is increased clearly, while the maximum power density of $Ni_{0.85}Cu_{0.15}$/SDC supported cell in this study is very close to the previous one. These results have clearly indicated good catalysis activities of $Ni_{1-x}Cu_x$/SDC anode with improved microstructure.

In order to investigate the effects of microstructure on the cell performance, typical electrochemical impedance spectra (EIS) have been measured at 600°C under open circuit conditions with a two-electrode configuration. The EIS Nyquist plots of three cells are shown in Fig. 5. On the left-hand side of the EIS Nyquist plot is the high high-frequency intercept, which represents the inherent ohmic resistance of the system. The polarization resistance of both anode and cathode, caused by polarization losses under operation, corresponds to the difference of the low and high frequency intercepts of the impedance spectrum with the real axis in the Nyquist plot [38]. It can be seen that the ohmic resistances of three cells are almost similar and the polarization resistances of $Ni_{0.9}Cu_{0.1}$/SDC, $Ni_{0.85}Cu_{0.15}$/SDC and $Ni_{0.8}Cu_{0.2}$/SDC supported cells are 0.22, 0.30 and 0.41 Ω cm^2, respectively. As aforementioned, all the anode/electrolyte substrates were manufactured under identical conditions, the cathodes of three cells were prepared with the same materials and processes, and the anode polarization resistance contributes to the low frequency part of the impedance measured with a tow-wire configuration [7]. Therefore, the differences in the polarization resistance are mainly caused by the anodic polarization resistance. One can see that the anodic polarization resistance is increased with decreasing of the hierarchical porous microstructure. The result shows that with optimized anode

microstructure the anode-electrolyte interface is improved and more effective TPBs are extended in the anode. Such an anode with the hierarchical porous microstructure can provide higher electrochemical and catalytic activity for CH_4 and improve stability of the CH_4-fueled SOFC.

3.3. Long-term stability and post-run analyses

The longer-term stability of an SOFC depends on the anode composition and structure when the hydrocarbon is used as fuel. In addition, the electrochemical reaction can only occur at the TPBs. The schematic of different anode TPBs are shown in Fig.6. During the operation of the cell, the continuous Ni atomic structure in the Ni-SDC anode leads to the formation of continuous carbon deposition on the TPBs and the carbon deposition is to cover the catalytically active Ni sites ultimately. However, in the $Ni_{1-x}Cu_x$/SDC anode, Cu addition can inhibit the continuous carbon deposition at TPBs between Cu, electrolyte and the fuel because Cu is relatively inert for carbon formation. Meanwhile, such TPBs can still provide activation for the fuel oxidation to produce steam, which can further enhance the tolerance to coking of $Ni_{1-x}Cu_x$-based anodes [39]. Therefore, the $Ni_{1-x}Cu_x$/SDC anodes possess great potential for long-running in IT-SOFCs fueled with dry methane.

In order to investigate the stability of the cells with different anodes for oxidation of dry CH_4, the time dependence of the power density of the three cells have been measured with a constant cell voltage of 0.5 V, shown in Fig. 7. As demonstrated in this figure, all the outputs of different anode-supported cells decrease versus operation time, but the difference clearly exists in the loss of total performance among these

cells as shown in Table 3. The total performance drop of the $Ni_{0.9}Cu_{0.1}$/SDC supported cell is only about 2.4% after 72h operation, which indicates that the $Ni_{0.9}Cu_{0.1}$/SDC is stable under the operating conditions in CH_4 atmosphere at 600 °C. However, the total performance drop of the $Ni_{0.85}Cu_{0.15}$/SDC supported cell and the $Ni_{0.8}Cu_{0.2}$/SDC supported cell has reached 6.9% and 14.5% respectively, indicating the $Ni_{1-x}Cu_x$/SDC anodes still suffer from the carbon poisoning with the decreased number of the hierarchical pores in these two anodes, although carbon deposition can be inhibited by increasing the addition of copper.

The impedance spectra measured at 600°C under open circuit conditions for three cells after 72h operation are shown in Fig. 8. Comparing with the initial ohmic resistance, there are almost no changes after 72h operation. The polarization resistance values of $Ni_{0.9}Cu_{0.1}$/SDC, $Ni_{0.85}Cu_{0.15}$/SDC and $Ni_{0.8}Cu_{0.2}$/SDC supported cells are 0.20, 0.34 and 0.52 Ω cm^2, respectively. The changes of polarization resistance are summarized in Table 3, from which one can see that the anodic polarization resistance of $Ni_{0.9}Cu_{0.1}$/SDC supported cell has decreased by 0.02 Ω cm^2, while other two have increased. This is caused by different carbon deposition rate of three cells during the operation with dry CH_4.

In order to investigate the carbon formation on the anode surface, EDS element mapping after electrical performance test has been carried out on these three anodes, shown in Fig. 9. It is clear that these anodes show different degrees of improved tolerance to coking under dry CH_4-fuelled operating conditions. It is believed that coking is caused by the deposition and absorption of carbon on the alloy surface and

the TPBs between alloy, electrolyte and fuel [39]. The $Ni_{0.9}Cu_{0.1}$/SDC supported cell shows least carbon deposition, which is uniformly distributed on its surface. Fewer coking can enhance the electronic conductivity and decrease the anode polarization resistance consequently. In contrast, there are larger amount of carbon deposited on the surface of $Ni_{0.8}Cu_{0.2}$/SDC anode and carbon clusters at the anode matrix. The deposited carbon blocks the anode pores and obstructs gas transportation, resulting in an increasing of the concentration polarization of the anode. Meanwhile, the covered TPBs lead to a decrease of the active site for fuel oxidation and increased the polarization resistance.

4. Conclusion

In summary, a uniform hierarchical porous $Ni_{1-x}Cu_x$ alloy-based anode has been developed through introducing a soluble pore former with the conventional fabrication techniques. It is found that the hierarchical porous microstructure is affected by the copper content in $Ni_{1-x}Cu_x$ alloy. Such an improved anode can promote gas transport and provide longer TPBs within the cell. The optimized $Ni_{0.9}Cu_{0.1}$/SDC anode with such microstructure shows exceptional performance and the corresponding cell exhibits a maximum power density of 379 mW cm^{-2} in dry CH_4 at 600°C. Durability test shows that there is only 2.4% power density drop after 72 h operation. These results have proved that the hierarchical porous microstructure can improve electrochemical and catalytic activities of $Ni_{1-x}Cu_x$ alloy-based anode and the long-term stability of CH_4-fueled SOFC operated at intermediate temperature.

Acknowledgments

This work is supported by National Natural Science Foundation of China (Grants No.11347023, No.11374043 and No.11174043), Natural Science Foundation of Jiangsu Educational Department (Grant No.15KJA430001), six-talent peak of Jiangsu Province (Grant No.2012-XCL-036), and Jiangsu student innovation and entrepreneurship training program (Grant No.201510333014Z).

5. References

[1] E.D. Wachsman, K.T. Lee, Lowering the Temperature of Solid Oxide Fuel Cells, Science 334 (2011) 935-939.

[2] B.C.H. Steele, A. Heinzel, Materials for fuel-cell technologies, Nature 414 (2001) 345-352.

[3] Y. Liu, C. Compson, M. Liu, Nanostructured and functionally graded cathodes for intermediate temperature solid oxide fuel cell, Journal of Power Sources 138 (2004) 194-198.

[4] J. Hou, F. Liu, Z. Gong, Y. Wu, W. Liu, Different ceria-based materials $Gd_{0.1}Ce_{0.9}O_{2-\delta}$ and $Sm_{0.075}Nd_{0.075}Ce_{0.85}O_{2-\delta}$ for ceria-bismuth bilayer electrolyte high performance low temperature solid oxide fuel cells, Journal of Power Sources 299 (2015) 32-39.

[5] A. M. Hussain, K.-J. Pan, I. A. Robinson, T. Hays, E. D. Wachsman. Stannate-Based Ceramic Oxide as Anode Materials for Oxide-Ion Conducting Low-Temperature Solid Oxide Fuel Cells, Journal of Electrochemical Society

163(2016) F1198-F1205.

[6] M.D. Gross, J.M. Vohs, R.J. Gorte, Recent progress in SOFC anodes for direct utilization of hydrocarbons, Journal of Materials Chemistry 17 (2007) 3071-3077.

[7] S. McIntosh, R.J. Gorte, Direct Hydrocarbon Solid Oxide Fuel Cells, Chemical Reviews 104(2004) 4845-4865.

[8] S. Park, J.M. Vohs, R.J. Gorte, Direct oxidation of hydrocarbons in a solid-oxide fuel cell, Nature 404 (2000) 265-267.

[9] K. Sasaki, K. Watanabe, K. Shiosaki, K. Susuki, Y. Teraoka, Multi-Fuel Capability of Solid Oxide Fuel Cells, Journal of Electroceramics 13 (2004) 669-675.

[10] A. Atkinson, S. Barnett, R. J. Gorte, J.T.S. Irvine, A.J.Mcevoy, M. Mogensen, S.C. Singhal, J.Vohs, Advanced anodes for high-temperature fuel cells, Nature Materials 5 (2004) 17-27.

[11] Y.S.H. Najjar, Hydrogen safety: The road toward green technology, International Journal of Hydrogen Energy 38 (2013) 10716-10728.

[12] S. Dutta, A review on production, storage of hydrogen and its utilization as an energy resource, Journal of Industrial and Engineering Chemistry 20 (2014) 1148-1156.

[13] S. Niaz, T. Manzoor, A.H. Pandith, Hydrogen storage: Materials, methods and perspectives, Renewable and Sustainable Energy Reviews 50 (2015) 457-469.

[14] R.M. Ormerod, Solid oxide fuel cells, Chemical Society Reviews 32 (2003) 17–28

[15] M. Boder, R. Dittmeyer, Catalytic modification of conventional SOFC anodes

with a view to reducing their activity for direct internal reforming of natural gas, Journal of Power Sources 155 (2006) 13-22.

[16] W.Z. Zhu, S.C. Deevi, A review on the status of anode materials for solid oxide fuel cells, Materials Science and Engineering A 362 (2003) 228-239.

[17] H. He, J.M. Vohs, R.J. Gorte, Carbonaceous deposits in direct utilization hydrocarbon SOFC anode, Journal of Power Sources 144 (2005) 135–140.

[18] J.B. Wang, J.C. Jang, T.J. Huang, Study of Ni-samaria-doped ceria anode for direct oxidation of methane in solid oxide fuel cells, Journal of Power Sources 122 (2003) 122–131.

[19] R.J. Gorte, S. Park, J.M. Vohs, C. Wang，Anodes for Direct Oxidation of Dry Hydrocarbons in a Solid-Oxide Fuel Cell，Advanced Materials 12 (2000) 1465-1469

[20] Z. Wang, W. Weng, K. Cheng, P. Du, G. Shen, G. Han, Catalytic modification of Ni–Sm-doped ceria anodes with copper for direct utilization of dry methane in low-temperature solid oxide fuel cells, Journal of Power Sources 179 (2008) 541-546.

[21] E.N. Armstrong, J.W. Park, N.Q. Minh, High-Performance Direct Ethanol Solid Oxide Fuel Cells, Electrochemical and Solid State Letters 15 (2012) B75-B77.

[22] Z. Liu, B. Liu, D. Ding, M. Liu, F. Chen, C. Xia, Fabrication and modification of solid oxide fuel cell anodes via wet impregnation/infiltration technique, Journal of Power Sources 237 (2013) 243-259.

[23] D.A. Osinkin, N.M. Bogdanovich, S.M. Beresnev, V.D. Zhuravlev, High-performance anode-supported solid oxide fuel cell with impregnated electrodes, Journal of Power Sources 288 (2015) 20-25.

[24] A. M. Hussain, J. V. T. Høgh, W. Zhang, P. Blennow, N. Bonanos, B. A. Boukamp, Effective improvement of interface modified strontium titanate based solid oxide fuel cell anodes by infiltration with nano-sized palladium and gadolinium-doped cerium oxide, Electrochimica Acta 113 (2013) 635-643.

[25] A. M. Hussain, J. V. T. Høgh, W. Zhang, N. Bonanos, Efficient ceramic anodes infiltrated with binary and ternary electrocatalysts for SOFCs operating at low temperatures, Journal of Power Sources 216 (2012) 308-313.

[26] Z. Xie, C. Xia, M.g Zhang, W. Zhu, H. Wang, $Ni_{1-x}Cu_x$ alloy-based anodes for low-temperature solid oxide fuel cells with biomass-produced gas as fuel, Journal of Power Sources 161 (2006) 1056-1061.

[27] C.M. Grgicak, M.M. Pakulska, J.S. O'Brien, J.B. Giorgi, Synergistic effects of $Ni_{1-x}Co_x$-YSZ and $Ni_{1-x}Cu_x$-YSZ alloyed cermet SOFC anodes for oxidation of hydrogen and methane fuels containing H_2S, Journal of Power Sources 183 (2008) 26-33.

[28] S. Song, M. Han，J. Zhang, H. Fan，NiCu–$Zr_{0.1}Ce_{0.9}O_{2-\delta}$ anode materials for intermediate temperature solid oxide fuel cells using hydrocarbon fuels，Journal of Power Sources 233 (2013) 62-68.

[29] H. Kim, C. Lu, W.L. Worrell, J.M. Vohs, R.J. Gorte, Cu-Ni Cermet Anodes for Direct Oxidation of Methane in Solid-Oxide Fuel Cells, Journal of The Electrochemical Society 149 (2002) A247-A250.

[30] C. Xia, W. Rauch, F. Chen, M. Liu, $Sm_{0.5}Sr_{0.5}CoO_3$ cathodes for low-temperature SOFCs, Solid State Ionics 149 (2002) 11-19.

[31] R. Tian, F. Zhao, F. Chen, C. Xia, Sintering of Samarium-doped ceria powders prepared by a glycine-nitrate process, Solid State Ionics 192 (2012) 580-583.

[32] Y. Zhang, S. Zha, M. Liu, Dual-Scale Porous Electrodes for Solid Oxide Fuel Cells from Polymer Foams, Advanced Materials 17 (2005) 487-491.

[33] T. Suzuki, Z. Hasan, Y. Funahashi, T. Yamaguchi, Y. Fujishiro, M. Awano, Impact of Anode Microstructure on Solid Oxide Fuel Cells, Science 325 (2009) 852-855.

[34] C. Ding, H. Lin, K. Sato, T. Kawada, J. Mizusaki, T. Hashida, Improvement of electrochemical performance of anode-supported SOFCs by NiO-$Ce_{0.9}Gd_{0.1}O_{1.95}$ nanocomposite powders, Solid State Ionics 181 (2010) 1238-1243.

[35] E.P. Murray, T. Tsai, S.A. Barnett, Adirect-methane fuel cell with a ceria-based anode, Nature 400 (1999) 649-651.

[36] J. Myung, T.H. Shin, X. Huang, G. Carins, J.T.S. Irvine, Enhancement of redox stability and electrical conductivity by doping various metals on ceria, $Ce_{1-x}MxO_{2-d}$ (M= Ni, Cu, Co, Mn, Ti, Zr), International Journal of Hydrogen Energy, 40 (2015) 12003-12008.

[37] T. Divya, N. K. Renuka, Modulated heterogeneous Fenton-like activity of 'M' doped nanoceria systems (M = Cu, Fe, Zr, Dy, La): Influence of reduction potential of doped cations, Journal of Molecular Catalysis A: Chemical 408(2015) 41-47.

[38] Q.A. Huang, R. Hui, B. Wang, J. Zhang, A review of AC impedance modeling and validation in SOFC diagnosis, Electrochimica Acta 52 (2007) 8144-8164.

[39] L. Yang, S. Wang, K. Blinn, M. Liu, Z. Liu, Z. Cheng, M. Liu, Enhanced Sulfur and Coking Tolerance of a Mixed Ion Conductor for SOFCs:

$BaZr_{0.1}Ce_{0.7}Y_{0.2-x}Yb_xO_{3-\delta}$, Science 326 (2009) 126-129.

Table 1 Porosity and conductivity of anodes after reduction with H_2 at 600 °C

Anodes	Porosity (%)	Conductivity at 600 °C (S/cm)
$Ni_{0.9}Cu_{0.1}$/SDC anode	41.6±2.8	435
$Ni_{0.85}Cu_{0.15}$/SDC anode	36.2±2.3	458
$Ni_{0.8}Cu_{0.2}$/SDC anode	32.4±1.9	491

Table 2 Open circuit voltages (OCVs) and maximum power densities (MPDs) for the $Ni_{1-x}Cu_x$/SDC supported cells operated at different temperature

$Ni_{1-x}Cu_x$/SDC supported cell	OCV (V)			MPD (mW cm^{-2})		
	550 °C	600 °C	650 °C	550 °C	600 °C	650 °C
$Ni_{0.9}Cu_{0.1}$	0.936	0.915	0.897	227	379	485
$Ni_{0.85}Cu_{0.15}$	0.921	0.894	0.871	192	337	437
$Ni_{0.8}Cu_{0.2}$	0.903	0.875	0.862	160	273	370

Table 3 Loss of power density and polarization resistance variations of anodes after 72h operation with dry CH_4

Anodes	Loss of power density (%)	Variation of polarization resistance (Ω cm^2)
$Ni_{0.9}Cu_{0.1}$/SDC anode	2.4	-0.02
$Ni_{0.85}Cu_{0.15}$/SDC anode	6.9	0.04
$Ni_{0.8}Cu_{0.2}$/SDC anode	14.5	0.11

Figure captions:

Fig. 1. XRD patterns of (a) $Ni_{0.9}Cu_{0.1}O$/SDC cermet and (b) $Ni_{0.9}Cu_{0.1}$/SDC anode.

Fig. 2. SEM images of (a) cross-sectional microstructure of a single $Ni_{0.9}Cu_{0.1}$/SDC anode-supported cell and (b) porous $Ni_{0.9}Cu_{0.1}$/SDC anode (the insert shows an enlargement of the smaller pores area)

Fig. 3. SEM images of cross-sectional microstructure (left) and EDS mapping of the copper distribution (right) of the $Ni_{1-x}Cu_x$/SDC anodes: (a) and (b) $Ni_{0.9}Cu_{0.1}$/SDC, (c) and (d) $Ni_{0.85}Cu_{0.15}$/SDC, (e) and (f) $Ni_{0.8}Cu_{0.2}$/SDC.

Fig. 4. Cell voltages (open symbols) and power densities (solid symbols) as function of current density of the $Ni_{1-x}Cu_x$/SDC supported cells tested at different temperatures: (a) $Ni_{0.9}Cu_{0.1}$/SDC supported cell, (b) $Ni_{0.85}Cu_{0.15}$/SDC supported cell and (c) $Ni_{0.8}Cu_{0.2}$/SDC supported cell.

Fig. 5. Impedance spectra measured at 600 °C under open circuit conditions for $Ni_{0.9}Cu_{0.1}$/SDC supported cell (square), $Ni_{0.85}Cu_{0.15}$/SDC supported cell (star) and $Ni_{0.8}Cu_{0.2}$/SDC supported cell (triangle) with dry CH_4 as fuel.

Fig. 6. Schematic of (a) Ni/SDC anode and (b) $Ni_{1-x}Cu_x$/SDC anode three-phase boundaries (TPBs).

Fig. 7. Power density of different anode-supported cells operated at 600°C with a constant cell voltage of 0.5 V and dry CH_4 as fuel.

Fig. 8. Impedance spectra measured at 600°C under open circuit conditions for $Ni_{0.9}Cu_{0.1}$/SDC supported cell (square), $Ni_{0.85}Cu_{0.15}$/SDC supported cell (star) and $Ni_{0.8}Cu_{0.2}$/SDC supported cell (triangle) with dry CH_4 as fuel after 72 h operation.

Fig. 9. EDS mapping of the carbon distribution on the different anodes surface: (a) $Ni_{0.9}Cu_{0.1}$/SDC, (b) $Ni_{0.85}Cu_{0.15}$/SDC, and (c) $Ni_{0.8}Cu_{0.2}$/SDC.

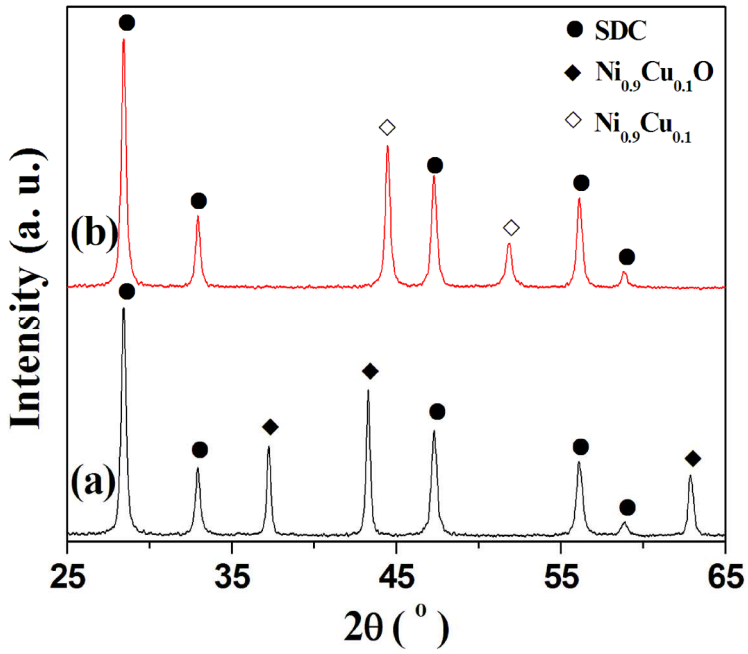

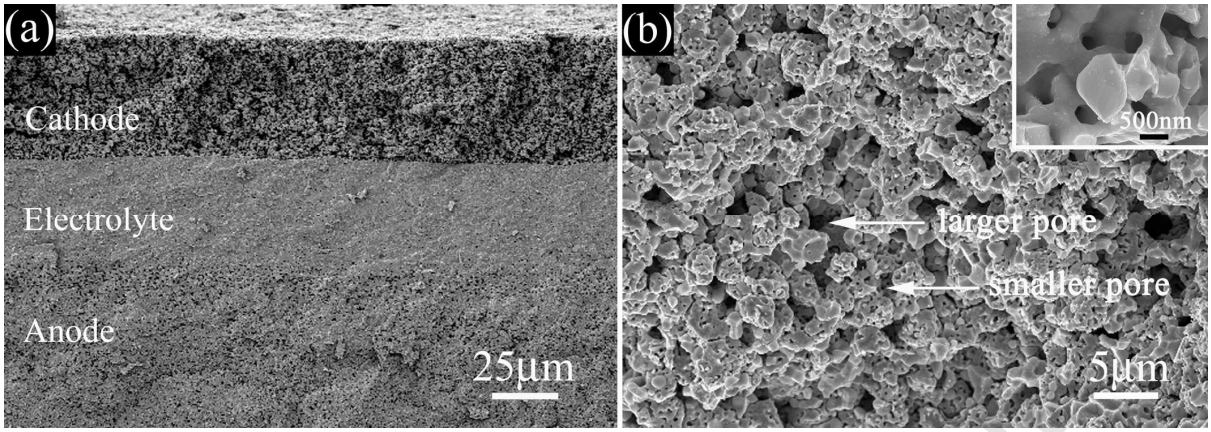

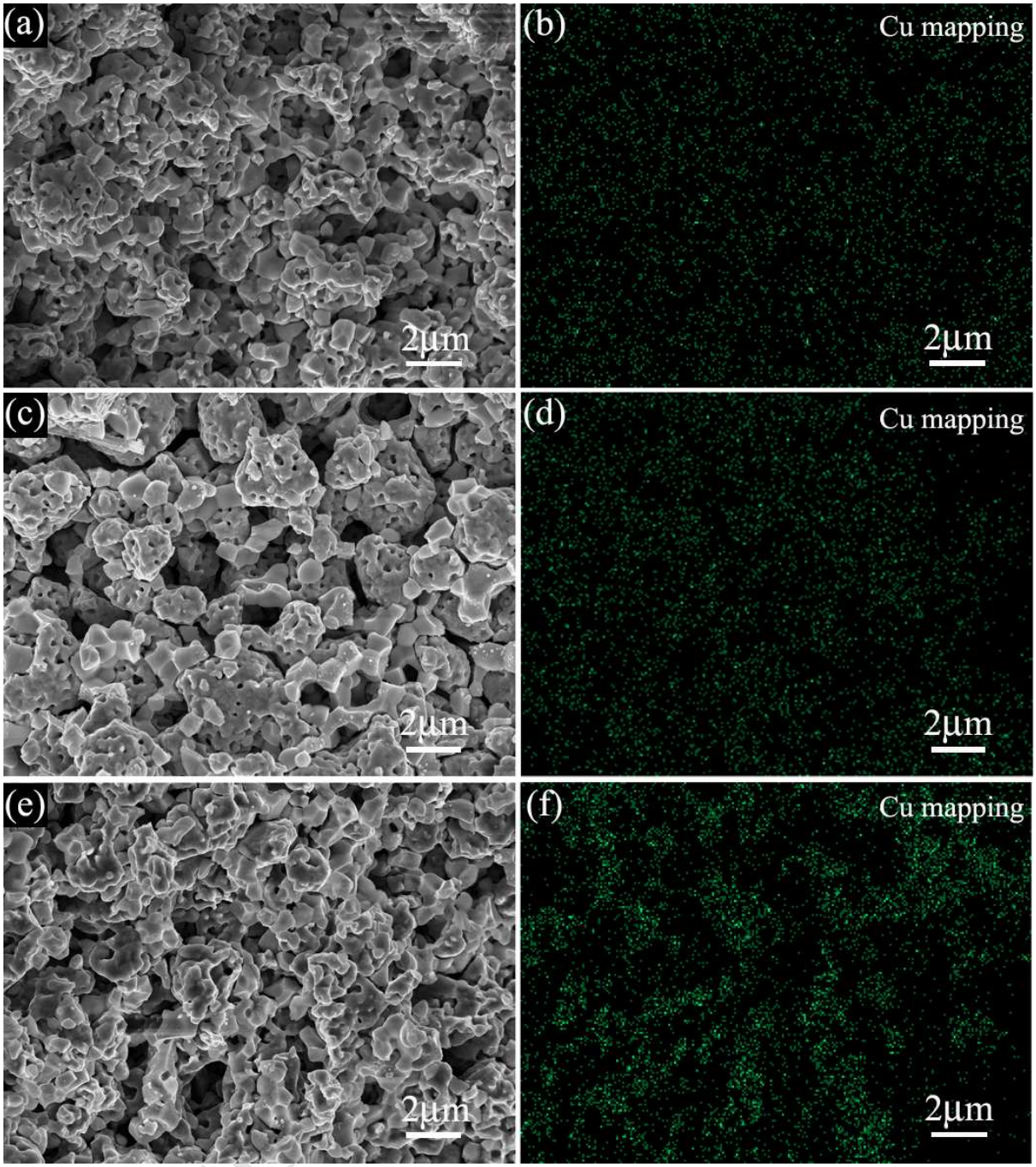
(a)
2μm
(b)
Cu mapping
2μm
(c)
2μm
(d)
Cu mapping
2μm
(e)
2μm
(f)
Cu mapping
2μm

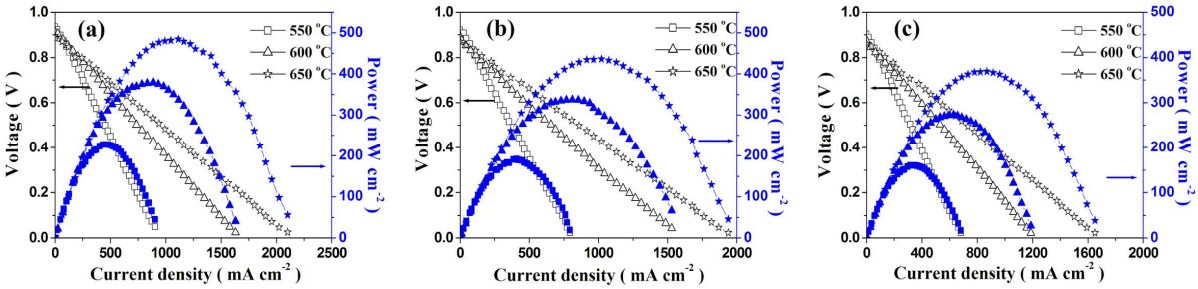

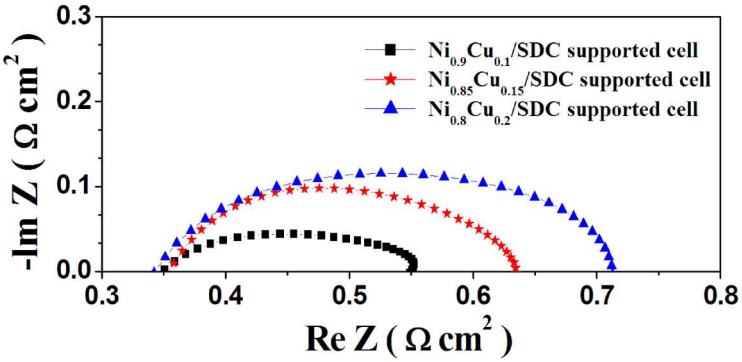

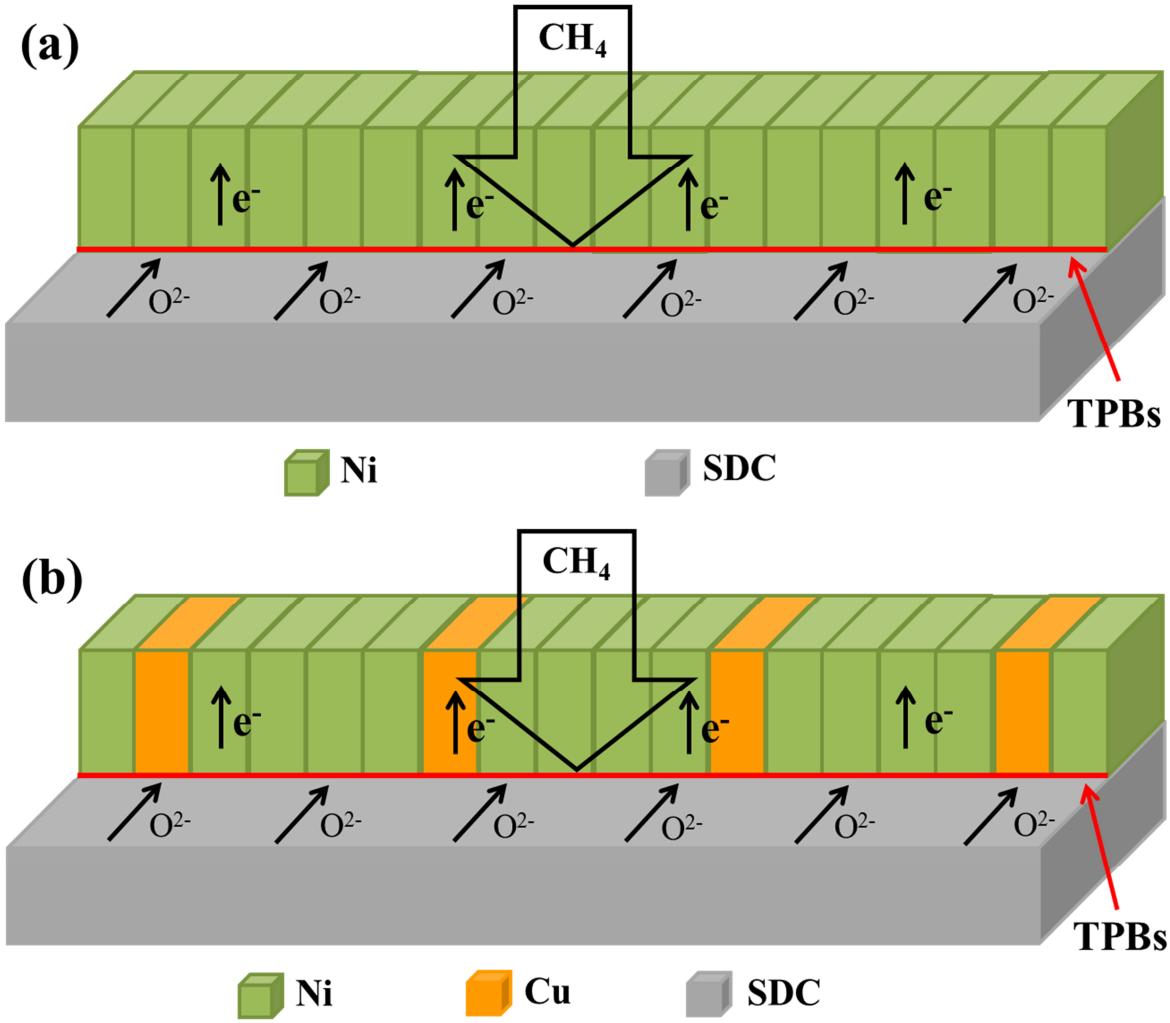
(a)
CH4
e-
e-
e-
e-
O2-
O2-
O2-
O2-
O2-
O2-
TPBs
Ni
SDC
(b)
CH4
e-
e-
e-
e-
O2-
O2-
O2-
O2-
O2-
O2-
TPBs
Ni
Cu
SDC

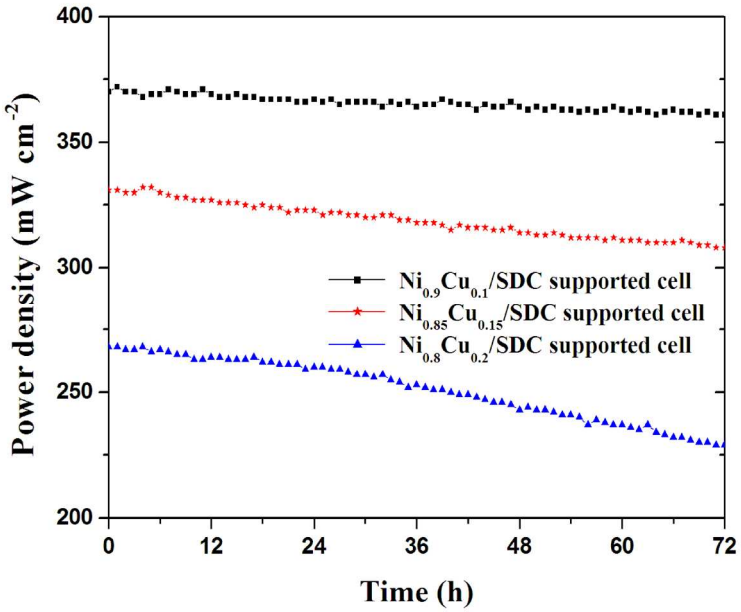

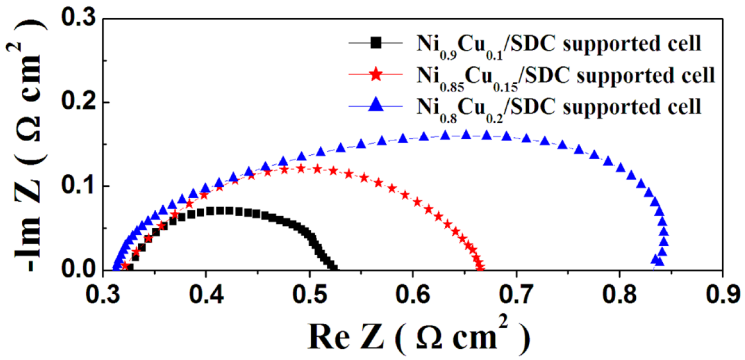

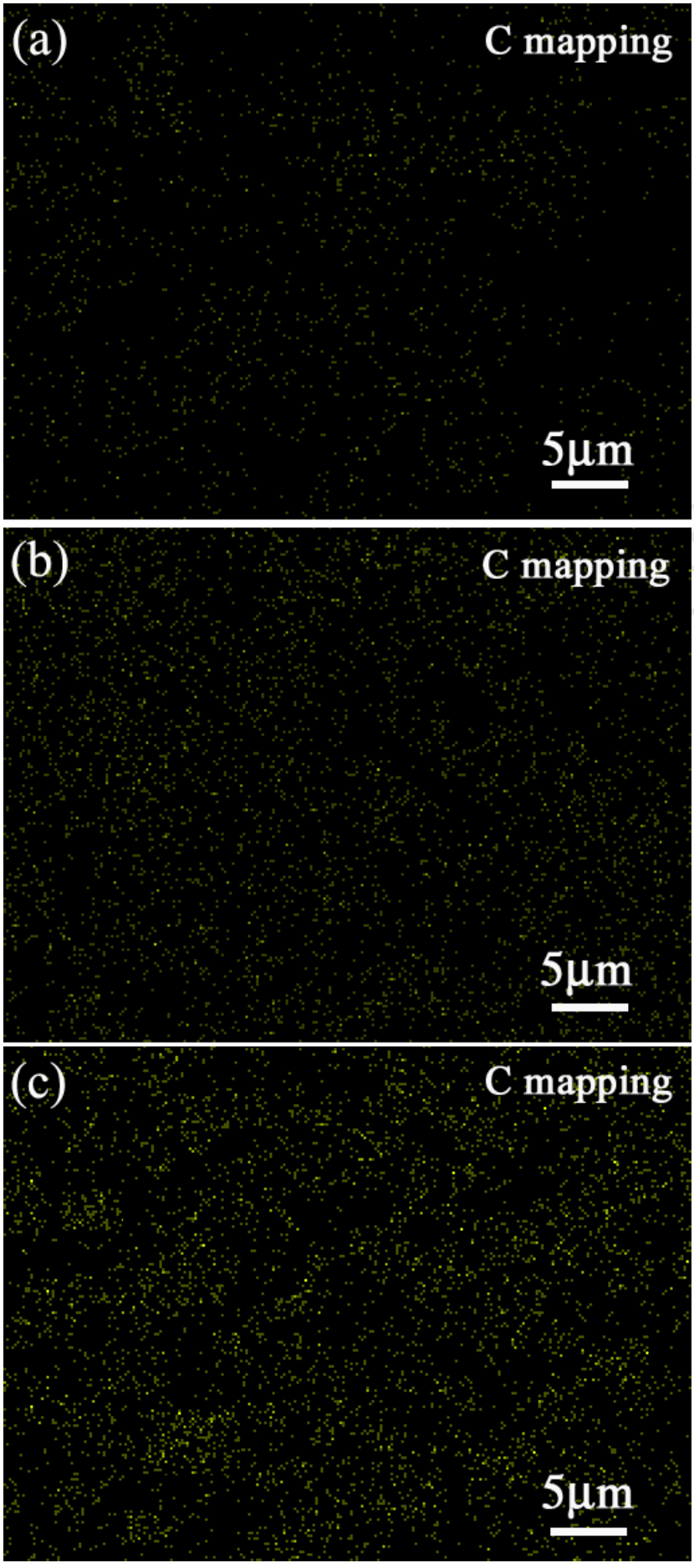
(a)
C mapping
5μm
(b)
C mapping
5μm
(c)
C mapping
5μm

Highlights

- A $Ni_{1-x}Cu_x$ alloy-based anode possessing a hierarchical porous structure was prepared.
- Such a novel anode was fabricated by co-pressing and co-sintering process.
- The smaller pores were homogeneously distributed in the anode matrix.
- The performance of the cell was improved with dry CH_4 fuel.
- Durability test showed only 2.4% power density drop after 72 h operation.